IEEE Access
Multidisciplinary ⋮ Rapid Review ⋮ Open Access Journal

Received November 13, 2017, accepted December 14, 2017, date of publication December 27, 2017, date of current version February 28, 2018.

Digital Object Identifier 10.1109/ACCESS.2017.2787732

A Novel Control Strategy for an Interior Permanent Magnet Synchronous Machine of a Hybrid Hydraulic Excavator

QIHUAI CHEN[1,2], TIANLIANG LIN[1], AND HAOLING REN[1]
[1]Huaqiao University, Xiamen 361021, China
[2]State Key Laboratory of Fluid Power and Mechatronic Systems, Zhejiang University, Hangzhou 310027, China

Corresponding author: Tianliang Lin (ltlkx1@163.com)

This work was supported in part by the National Natural Science Foundation of China under Grant 51505160, in part by the Natural Science Foundation of Fujian Province under Grant 2017J01087, in part by the Open Foundation of the State Key Laboratory of Fluid Power and Mechatronic Systems under Grant GZKF-201611, and in part by the China Postdoctoral Science Foundation under Grant 2017M612139.

ABSTRACT A hybrid power train system, which uses an electric machine to balance fluctuations of a load, is a practicable method to improve the efficiency of hydraulic excavators. To realize fast charge and discharge, ultra-capacitors are applied to a hybrid hydraulic excavator (HHE), which will cause the direct current (dc) supply voltage to change in a wide range. When the voltage of the ultra-capacitor varies, the output torque of the electric machine will be affected. In this paper, an interior permanent magnet synchronous machine (IPMSM) is employed in the HHE. When the dc supply voltage is low, the output torque of the IPMSM will drop and cannot balance fluctuations of the load adequately. To improve the control performance of the IPMSM output torque, a novel high-performance control strategy based on a vector control is proposed for the IPMSM to reduce the influence from the dc voltage. The mutual influence between the torque of the IPMSM and the dc voltage is analyzed. The novel high-performance control strategy for the IPMSM is introduced. To verify the effectiveness of the novel control strategy for the IPMSM, simulations and experiments are carried out. The results show that the proposed control strategy can improve the control performance of the IPMSM.

INDEX TERMS Energy conservation, hybrid power train system, hybrid hydraulic excavator, interior permanent magnet synchronous machine, vector control.

I. INTRODUCTION

Excavators are widely used in various earthworks. However, the efficiency of the excavator is always unsatisfactory [1]. A hybrid power train system (HPTS) which makes use of an electric machine to balance fluctuations of a load and stabilizes working points of an engine in high efficiency area, is a practical method to improve the efficiency of the hydraulic excavator [2]–[4].

A typical HPTS schematic is given in Fig. 1 [5]. The load profile measured from a 20 ton excavator in five typical working cycles is given in Fig. 2. As can be found, the load of the excavator changes violently. In a hybrid hydraulic excavator (HHE), to realize fast charge and discharge, ultra-capacitors are applied [6], which will cause the direct current (DC) supply voltage to change in a wide range. While, the HHE uses the ultra-capacitor to supply the electric machine directly, which will affect the output torque of the electric machine [7]. Therefore, an appropriate control strategy for the electric machine to make its torque insensitive to the influence from the DC voltage is significant. A lot of researches have been done to improve the system control performance [8]–[14].

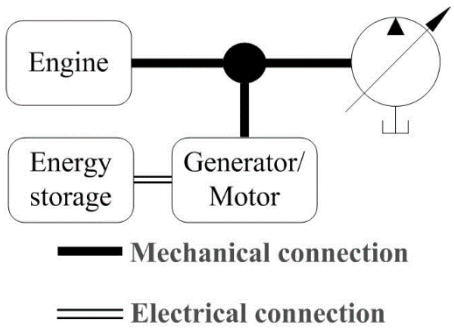

FIGURE 1. The HPTS schematic.

A permanent magnet synchronous machine (PMSM) which is high efficiency, high power density, easy control and good field weakening control [15], is an ideal candidate for

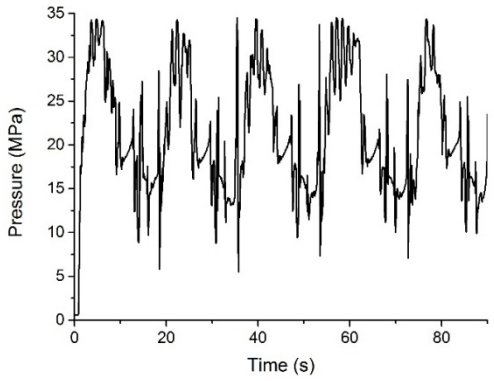

FIGURE 2. The load profile of a 20 ton excavator.

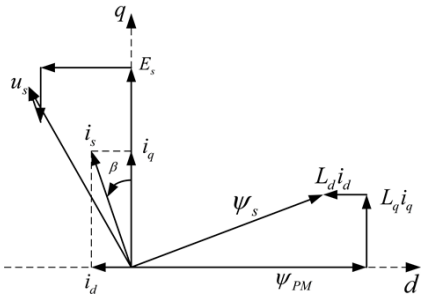

FIGURE 3. The electric vector diagram of the IPMSM.

the HHE. According to the research status of the PMSM at home and abroad, to control the PMSM, the field oriented control in the rotor synchronous (d-q) frame [16], [17], direct torque control and direct flux vector control [18], [19] in the flux linkage synchronous (f-t) frame [20]–[22] are studied. Compared with the direct torque control and the direct flux vector control, the d-q frame based control decoupled the PMSM magnetic field and is not dependent on the real-time parameters of the PMSM. In order to control the PMSM operating at the optimal efficiency area, the maximum torque control [23], [24] is proposed in constant torque region.

In the HHE, due to the usage of ultra-capacitors, the DC supply voltage varies in a wide range. When the voltage of the ultra-capacitor is low, the output torque of the PMSM will drop and cannot balance the fluctuation of the load adequately. In this article, a novel high performance control strategy for an interior PMSM (IPMSM) in the HHE is proposed to improve its torque controllability and to make it insensitive to the influence from DC voltage. This article is organized as follows. The influence from the DC voltage is analyzed in section ''Preliminary analysis''. A novel control strategy for the IPMSM in the HHE is presented in section ''High performance control strategy''. The design of the controller for the IPMSM is shown in section ''Controller design''. Simulation research is given in section ''Simulation research''. Some experiments are carried out and shown in section ''Experimental research''. Concluding remarks are drawn in section ''Conclusion''.

II. PRELIMINARY ANALYSIS

In order to analyze the influence from the DC voltage on the output torque of an IPMSM in the HHE, the IPMSM should be investigated firstly. The electrical vector diagram is shown in Fig. 3. The mathematical model of the IPMSM drive system in d-q coordinate system can be given as

$$\begin{cases} u_d = R_a i_d + L_d \dfrac{di_d}{dt} - w_e L_q i_q \\ u_q = w_e L_d i_d + R_a i_q + L_q \dfrac{di_q}{dt} + w_e \Psi_{pm} \end{cases} \tag{1}$$

$$T = \frac{3}{2} p(\psi_{PM} i_s \cos\beta - \frac{1}{2}(L_d - L_q) i_s^2 \sin(2\beta)) \tag{2}$$

where, u_s is the stator voltage. E_s is the back electromotive force. u_d and u_q are the stator voltages of d-axis and q-axis, respectively. w_e is the electric angular velocity. i_s is the stator current. i_d and i_q are the stator current of d-axis and q-axis, respectively. L_d and L_q are the inductance of d-axis and q-axis, respectively. Ψ_{pm} is the flux linkage produced by the permanent magnet. Ψ_s is the flux linkage produced by the winding. R_a is the stator resistance. T is the output torque of the IPMSM. p is the number of the pole pairs. β is the torque angle.

To improve the efficiency of the IPMSM, the maximum torque vector control is employed. According to the vector diagram, the stator current of d-axis and q-axis can be described as

$$\begin{cases} i_d = -i_s \sin\beta \\ i_q = i_s \cos\beta \end{cases} \tag{3}$$

The maximum torque control condition can be obtained according to

$$\frac{\partial T}{\partial \beta} = 0 \tag{4}$$

The maximum torque control condition can be described as

$$\sin\beta = \frac{\Psi_{pm} - \sqrt{\Psi_{pm} + 8(L_d - L_q)^2 i_s^2}}{4(L_d - L_q) i_s} \tag{5}$$

By substituting (5) into (3), the stator current of d-axis and q-axis corresponding to the maximum torque control can be acquired as

$$i_d = \frac{\Psi_{pm}}{2(L_q - L_d)} - \sqrt{\frac{\Psi_{pm}^2}{4(L_q - L_d)^2} + i_q^2} \tag{6}$$

The stator current trajectory of d-axis and q-axis based on the maximum torque control can be plotted as Fig. 4.

The HHE uses the ultra-capacitor as the energy storage unit. The DC voltage changes in real time. Meanwhile, each component in the IPMSM control system is restricted by their carrying capacity. Therefore, in the control of the stator current of d-axis and q-axis, the DC voltage and the inverter carrying capacity constraints should be considered.

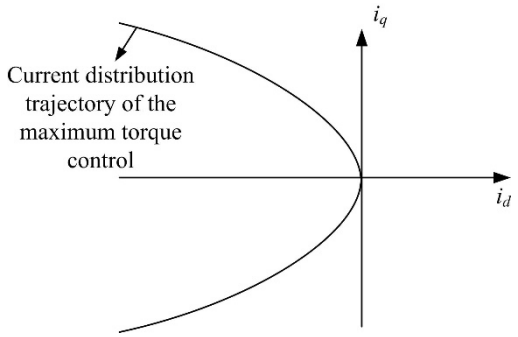

FIGURE 4. The stator current trajectory of the maximum torque control.

The current and the voltage constraints of the IPMSM can be expressed as

$$|i_s| = \sqrt{i_d^2 + i_q^2} \le i_{s\max} \tag{7}$$

$$|u_s| = \sqrt{u_d^2 + u_q^2} \le u_{s\max} \tag{8}$$

where, $i_{s\max}$ (>0) is the maximum phase current, which is decided by the inverter and the IPMSM. $u_{s\max}$ (>0) is the maximum phase voltage, which is decided by the ultra-capacitor DC voltage.

Substituting (1) into (8), and ignoring the influence of the stator resistance, the steady state of the voltage constraint can be re-expressed as

$$(i_d + \frac{\Psi_{pm}}{L_d})^2 + (\frac{L_q}{L_d})^2 i_q^2 \le (\frac{u_{s\max}}{L_d w_e})^2 \tag{9}$$

As can be seen, the current constraint is a circle. The radius and the center of the current constraint are $i_{s\max}$ and the origin of the d-q coordinate system, respectively. Besides, they are fixed. The voltage constraint is an ellipse. The center of the ellipse is $(-\psi_{pm}/L_d, 0)$ and it is fixed. While, the radius of the ellipse decreases with the reduction of the DC voltage and the increase of the rotary speed.

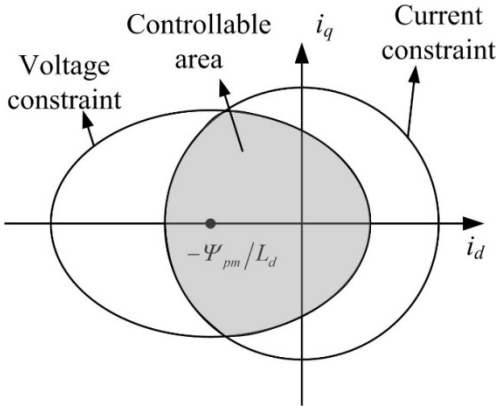

FIGURE 5. Current and voltage constraints curve and IPMSM controllable area in *d-q* coordinate system.

The constraints of the voltage and the current are defined as sets $\boldsymbol{U}$ and $\boldsymbol{I}$. The controllable sets of the IPMSM are $\boldsymbol{U} \cap \boldsymbol{I}$, which can be expressed as in Fig. 5. Therefore, the controllable area of the IPMSM is decided by the current constraint as well as the voltage constraint synchronously. The current constraint is fixed. While, the voltage constraint is varied with the DC voltage and the rotary speed.

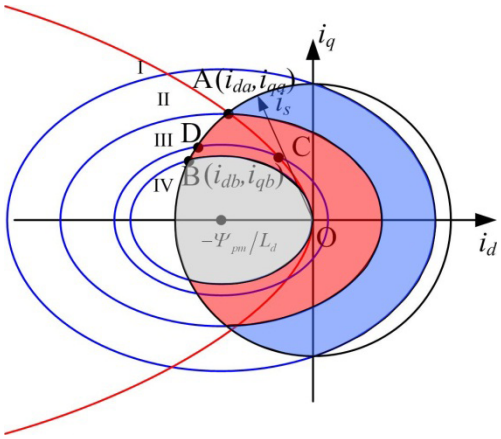

FIGURE 6. Constraints curves and the stator current trajectory of the maximum torque control.

III. HIGH PERFORMANCE CONTROL STRATEGY FOR THE IPMSM

In the HHE, the IPMSM works in the generator mode and the motor mode. The control strategy of the generator mode is similar to that of the motor mode. The control for the IPMSM in generator mode only needs to change the sign of i_q. When $i_q > 0$, the IPMSM works in the motor mode. When $i_q < 0$, the IPMSM works in the generator mode. Besides, the current constraint and the voltage constraint are d axisymmetric. Therefore, the motor mode is taken into consideration in the following analysis. An assumption that the IPMSM can be controlled, which is $\boldsymbol{U} \cap \boldsymbol{I} \neq \emptyset$ is made. According to (9), critical voltage constraints varied with w_e and $u_{s\max}$ can be acquired. Combined with the stator current trajectory of the maximum torque control, constraints of different voltages and current can be re-plotted in Fig. 6. The black curve is the current constraint. The blue curves are voltage constraints of different DC supply voltages. The red curve is the stator current trajectory of the maximum torque control. The point A (i_{da}, i_{qa}) is the intersection of the stator current trajectory of the maximum torque control and the current constraint. The point B (i_{db}, i_{qb}) is the intersection of the voltage constraint and the current constraint, when the voltage constraint passes through the origin O in d-q coordinate. In an established IPMSM control system, points A and B are both fixed and available. The d-q current components of the point A can be calculated as

$$\begin{cases} i_{da} = \dfrac{\Psi_{pm}}{2(L_q - L_d)} - \sqrt{\dfrac{\Psi_{pm}^2}{4(L_q - L_d)^2} + i_{qa}^2} \\ i_{s\max} = \sqrt{i_{da}^2 + i_{qa}^2} \end{cases} \tag{10}$$

Similarly, the d-q current components of point B can be calculated as

$$\begin{cases} (i_{db} + \frac{\Psi_{pm}}{L_d})^2 + (\frac{L_q}{L_d})^2 i_{qb}^2 = (\frac{\Psi_{pm}}{L_d})^2 \\ i_{s\max} = \sqrt{i_{db}^2 + i_{qb}^2} \end{cases} \tag{11}$$

where, i_{da} and i_{qa} are d axis and q axis current components of point A. i_{db} and i_{qb} are d axis and q axis current components of point B.

As can be seen in Fig. 6, with the variation of the DC voltage supply, the controllable area of the IPMSM will shrink. Combined with the maximum torque control, the controllable area of the IPMSM can be divided into three working conditions. They are maximum torque controllable region, local maximum torque controllable region and maximum torque uncontrollable region, respectively.

The maximum torque controllable region corresponds to the blue part in Fig. 6. In this region, the DC supply voltage is large enough. The d-q current components controlled through the maximum torque control is not restricted by the DC supply voltage. The DC supply voltage in this region should satisfy (12).

$$(i_{da} + \frac{\Psi_{pm}}{L_d})^2 + (\frac{L_q}{L_d})^2 i_{qa}^2 \le (\frac{u_s}{L_d w_e})^2 \tag{12}$$

The desired d-q current components can be calculated from

$$\begin{cases} T = \dfrac{3}{2} p(\psi_{PM} i_q + (L_d - L_q) i_d i_q) \\ i_d = \dfrac{\Psi_{pm}}{2(L_q - L_d)} - \sqrt{\dfrac{\Psi_{pm}^2}{4(L_q - L_d)^2} + i_q^2} \end{cases} \tag{13}$$

The command trajectory of d-q current components in this region is an arc segment from O to A. The maximum torque in this region can be calculated according to the d-q current components of point A.

The local maximum torque controllable region corresponds to the red part in Fig. 6. In this region, the d-q current components controlled through the maximum torque control is constrained by the DC supply voltage. The DC supply voltage in this region should satisfy (14).

$$\begin{aligned} (i_{db} + \frac{\Psi_{pm}}{L_d})^2 + (\frac{L_q}{L_d})^2 i_{qb}^2 &\le (\frac{u_s}{L_d w_e})^2 \\ &\le (i_{da} + \frac{\Psi_{pm}}{L_d})^2 + (\frac{L_q}{L_d})^2 i_{qa}^2 \end{aligned} \tag{14}$$

In this region, only part of the target torque can be controlled by maximum torque control. Curve III is a typical voltage constraint in this region. The desired d-q current components which the maximum torque control can be used is distributed on an arc segment from O to C. The maximum torque can be controlled through the maximum torque control happens to point C and it can be calculated as

$$\begin{cases} i_{dc} = \dfrac{\Psi_{pm}}{2(L_q - L_d)} - \sqrt{\dfrac{\Psi_{pm}^2}{4(L_q - L_d)^2} + i_{qc}^2} \\ (i_{dc} + \dfrac{\Psi_{pm}}{L_d})^2 + (\dfrac{L_q}{L_d})^2 i_{qc}^2 = (\dfrac{u_{sIII}}{L_d w_e})^2 \\ T_c = \dfrac{3}{2} p(\psi_{PM} i_{qc} + (L_d - L_q) i_{dc} i_{qc}) \end{cases} \tag{15}$$

where, u_{sIII} is the voltage vector magnitude of the curve III. T_c is the maximum torque which can be controlled through the maximum torque control. When the desired torque is smaller than T_c. The desired torque can be obtained by using the maximum torque control and it can be calculated according to the (13). While, when the desired torque is larger than the maximum torque controlled by the maximum torque control, the maximum torque control cannot be applied due to the low DC supply voltage. The maximum torque in this region can be obtained according to the d-q current components of point D and it can be calculated as

$$\begin{cases} (i_{dd} + \dfrac{\Psi_{pm}}{L_d})^2 + (\dfrac{L_q}{L_d})^2 i_{qd}^2 = (\dfrac{u_{sIII}}{L_d w_e})^2 \\ i_{s\max} = \sqrt{i_{dd}^2 + i_{qd}^2} \\ T = \dfrac{3}{2} p(\psi_{PM} i_{qd} + (L_d - L_q) i_{dd} i_{qd}) \end{cases} \tag{16}$$

where, i_{dd} and i_{qd} is the d-q current components of the point D, respectively.

The maximum torque uncontrollable region corresponds to the grey part in Fig. 6. The DC supply voltage in this region should satisfy (17).

$$(\frac{u_s}{L_d w_e})^2 \le (i_{db} + \frac{\Psi_{pm}}{L_d})^2 + (\frac{L_q}{L_d})^2 i_{qb}^2 \tag{17}$$

In this region, the maximum torque control cannot be used. The maximum torque in this region can be obtained according to the d-q current components of the intersection of the current constraint and the voltage constraint and it can be calculated as

$$\begin{cases} (i_d + \dfrac{\Psi_{pm}}{L_d})^2 + (\dfrac{L_q}{L_d})^2 i_q^2 = (\dfrac{u_{sIV}}{L_d w_e})^2 \\ i_{s\max} = \sqrt{i_d^2 + i_q^2} \\ T = \dfrac{3}{2} p(\psi_{PM} i_q + (L_d - L_q) i_d i_q) \end{cases} \tag{18}$$

where, u_{sIV} is the low DC supply voltage distributed in the maximum torque uncontrollable region.

In the local maximum torque controllable region and the maximum torque uncontrollable region, when the maximum torque control cannot be employed, in order to extend the working range of the IPMSM under the conditions of low DC supply voltage, an appropriate flux weakening control should be used for the IPMSM. At this time, according to the different DC supply voltage, the desired d-q current components

based on the target torque can be calculated as

$$\begin{cases} (i_d + \dfrac{\Psi_{pm}}{L_d})^2 + (\dfrac{L_q}{L_d})^2 i_q^2 = (\dfrac{u_{sIV}}{L_d w_e})^2 \\ i_{s\max} = \sqrt{i_d^2 + i_q^2} \\ T = \dfrac{3}{2} p(\psi_{PM} i_q + (L_d - L_q) i_d i_q) \end{cases} \tag{19}$$

Based on the above analysis, the control principle of the IPMSMS can be extracted. The control flow chart is given in Fig. 7.

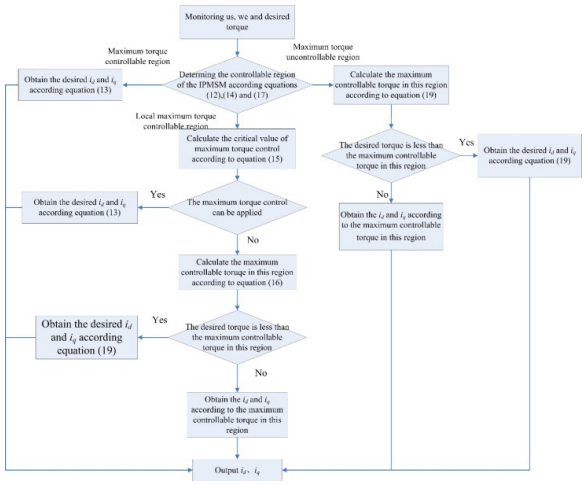

FIGURE 7. The control flow chart of the IPMSM.

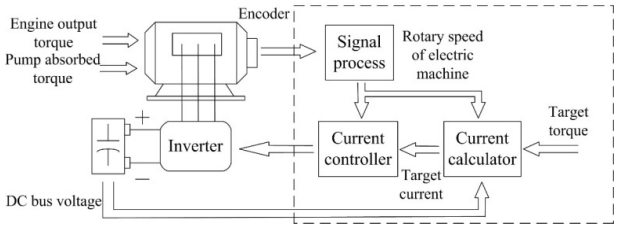

FIGURE 8. The control system structure diagram of the IPMSM.

IV. CONTROLLER DESIGN

The control system structure diagram of the IPMSM in the HHE can be described in Fig. 8. As can be seen, the mechanical inputs of the IPMSM come from the engine and the pump. The control part of the IPMSM is given in the dashed frame. The control part consists of three parts, they are signal process, current calculator and current controller. To control the power inverter, a SVPWM is adopted.

The transfer function of the power inverter can be treated as a first order inertial link and can be expressed as

$$G_{inv}(s) = \frac{K_{inv}}{T_{inv}s + 1} \tag{20}$$

where, K_{inv} is the gain of the power inverter. T_{inv} is the time constant of the power inverter.

In the torque controller, a current closed-loop control is adopted. The phase current of the IPMSMS is detected by Hall sensors. Considering the delay caused by signal acquisition and filtering in the current feedback process, the current feedback link can be denoted as a first order inertial link and expressed as

$$G_{if}(s) = \frac{1}{T_{if}s + 1} \tag{21}$$

where, T_{if} is the time constant of the current feedback link.

To control the torque of the IPMSM in the HHE, a PI controller is employed. Meanwhile, in order to solve the problem that the IPMSM cannot be completely decoupled due to the back electromotive force, a feedforward compensation control is used in the current control process. According to the electric angular velocity, IPMSM parameters and control parameters, the back electromotive force in the IPMSM control process is calculated and compensated at the output of the PI controller. The controller of the IPMSM is given in Fig. 9.

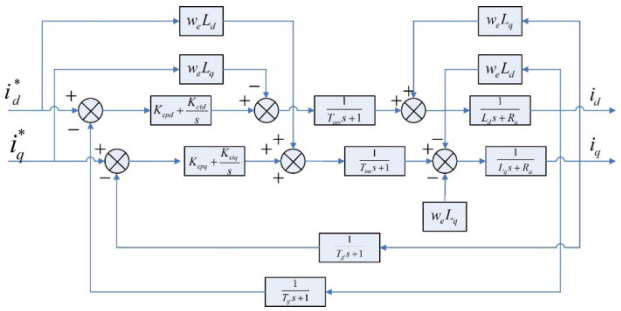

FIGURE 9. The controller of the IPMSM.

The implementation algorithm of the PI controller can be described as

$$u_d = (i_d^* - i_d)\left(K_{cpd} + \frac{K_{cid}}{s}\right) - \omega_e L_q i_q^* \tag{22}$$

$$u_q = \left(i_q^* - i_q\right)\left(K_{cpq} + \frac{K_{ciq}}{s}\right) + \omega_e L_d i_d^* + \omega_e \psi_f \tag{23}$$

where, i_d^* is the desired d axis current component, i_q^* is the desired q axis current component, K_{cpd} is the gain of the PI controller of d axis, K_{cid} is the integral coefficient of the PI controller of d axis. K_{cpq} is the gain of the PI controller of q axis, K_{ciq} is the integral coefficient of the PI controller of q axis.

According to the Fig. 9, the system open loop transfer function can be expressed as

$$G_{co}(s) = \frac{k_{cp}s + k_{ci}}{s(Ls + R_a)(T_{inv}s + 1)\left(T_{if}s + 1\right)} \tag{24}$$

where, L is the d axis or q axis inductance of the IPMSM, K_{cp} is the gain of the PI controller of d axis or q axis. K_{ci} is the integral coefficient of the PI controller of d axis or q axis. In the IPMSM, the machine time constant is far greater than the inverter time constant and the current feedback link time constant. Therefore, in order to broaden the bandwidth of

the IPMSM controller, the zero pole cancellation method is employed to reduce the impact of the large time constant. The parameters of the PI controller can be obtained as

$$K_{cp}/K_{ci} = L/R_a \tag{25}$$

Then the closed-loop transfer function of the IPMSM control system can be described as

$$G_{cc}(s) = \frac{K_{cp}\left(T_{if}s+1\right)}{LT_{inv}T_{if}s^3 + L\left(T_{inv}+T_{if}\right)s^2 + Ls + K_{cp}} \tag{26}$$

In (26), the inverter time constant and the current feedback link time constant are so small that the influence of the three order term can be neglected. Therefore, the control system can be considered as a two order system. According to the best requirement of the damping ratio of a two order system, the ratio coefficients of the PI controller need to satisfy the following relation.

$$\xi_{cc} = \frac{1}{2}\sqrt{\frac{L_s}{K_{cp}\left(T_{inv}+T_{if}\right)}} = \frac{\sqrt{2}}{2} \tag{27}$$

where, ξ_{cc} is the damping ratio of the controller. Similarly, the integral coefficient of the PI controller can be obtained as

$$K_{cp} = \frac{L}{2\left(T_{inv}+T_{if}\right)} \tag{28}$$

$$K_{ci} = \frac{R_a}{2\left(T_{inv}+T_{if}\right)} \tag{29}$$

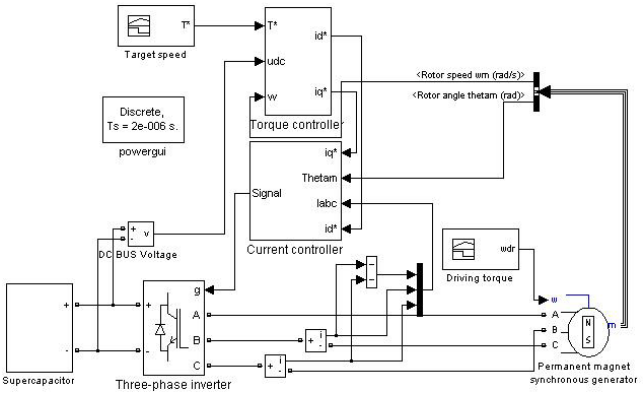

FIGURE 10. The IPMSM in the HHE simulation diagram.

V. SIMULATION RESEARCH

To validate the effectiveness of the control system, the simulations are carried out in Simulink. In the HHE, the engine and the hydraulic pump can be treated as the drive (or load) speed module of the IPMSM. Therefore, the model of the IPMSM in the HHE is shown in Fig. 10. As can be seen, the model consists of five parts. They are the IPMSM, the inverter, the torque controller, the current controller and the signals acquisition, respectively. The high performance control strategy is realized in the torque controller. The feedforward compensation PI control is achieve in the current controller. The parameters of the IPMSM is given in Table 1.

TABLE 1. Parameters of the IPMSM.

Quantity	Value[a]
Rating speed	1800 rpm
Rating torque	200 Nm
Pole pairs	3
Stator resistor	0.0417 Ω
Flux linkage	0.249 Vs
Inductance of d axis	0.912 mH
Inductance of q axis	1.3 mH
Ultra-capacitor capacity	12 F

In order to facilitate the comparison, the traditional vector control is also simulated. For different DC supply voltages, the input torque signal of the IPMSM is 200 Nm. The output torque of the IPMSM in simulation model by using the traditional vector control are given in Fig. 11. As can be seen, with the decrease of the DC supply voltage, the controllability of the IPMSM is becoming worse.

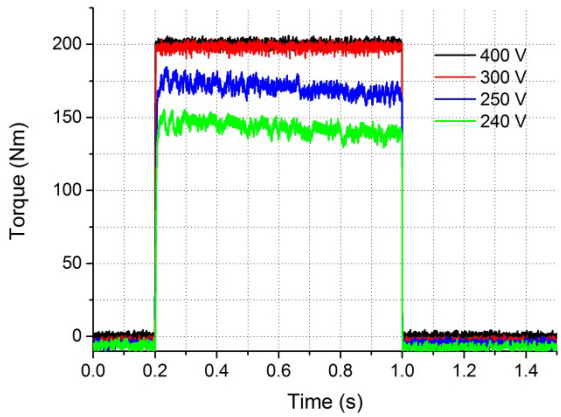

FIGURE 11. The output torque of the IPMSM by using traditional vector control.

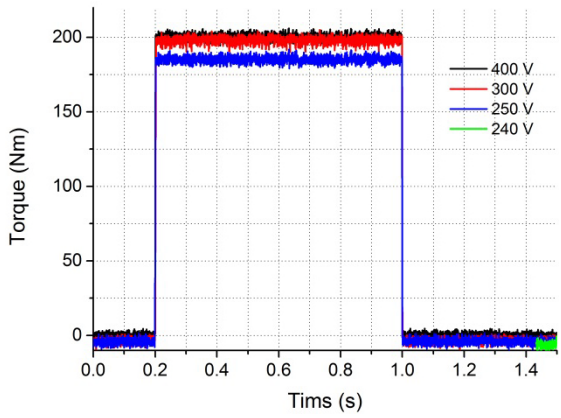

FIGURE 12. The output torque of the IPMSM by using high performance control strategy.

The output torque of the IPMSM in simulation model by using the high performance control strategy are given in Fig. 12. As can be seen, the high performance control

strategy can effectively guarantee the control performance of the IPMSM.

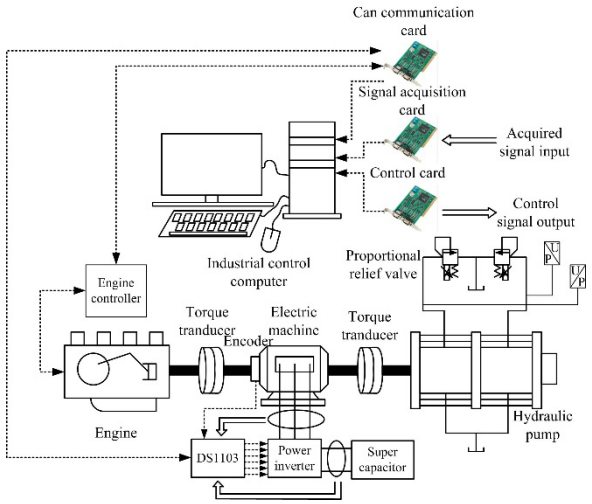

FIGURE 13. The schematic diagram of the HPTS test platform.

VI. EXPERIMENTAL RESEARCH

Relevant experimental studies are also carried out for the proposed control strategy. A HPTS of the HHE loading test platform is built. The schematic diagram of the test platform is shown in Fig. 13. In the experimental platform, an engine, an electric machine and a hydraulic pumps are coaxially connected. Two torque sensors are armed to detect the torque of the engine and the pump. An Advantech IPC is used to control the platform. The engine is controlled by an engine controller. Each controller is communicated through CAN communication protocol. Meanwhile, the hydraulic pump and the loading proportional relief-valves are controlled by Advantech IPC control cards. The signals of the output torque of the engine, the absorbed torque of the hydraulic pump, the output pressure of the hydraulic pump, the current and the voltage of the ultra-capacitor is acquired by Advantech IPC acquisition cards.

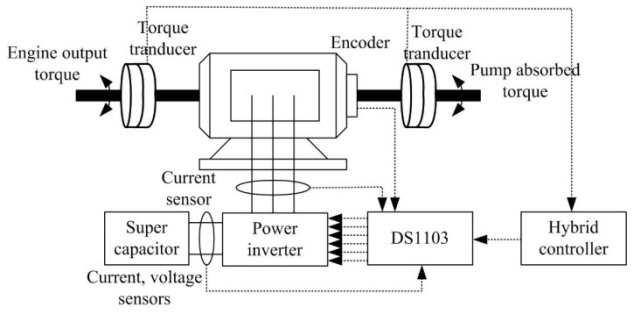

FIGURE 14. The schematic diagram of the IPMSM control system.

The schematic diagram of the IPMSM control system is given in Fig. 14. The proposed control strategy is realized in a dSPACE1103 digital signal processor. An encoder, voltage sensors and current sensors are used to detect the rotary speed, DC supply voltage, phase current and DC current in the process of the running of the IPMSM. The part of the platform is given in Fig. 15. The main components parameters of the experimental platform are given in Table 2.

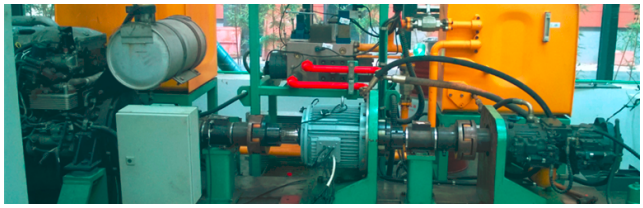

FIGURE 15. The part of the experimental platform.

TABLE 2. Main component parameters in the HPTS.

Component	Model (Parameters)[a]
Engine	Mistubishi 4M5O-TLU3C
Auxiliary power unit	PMSM 38 kW (self-developed)
Hydraulic pump	Kawasaki K3V 112 DT-1CE R-9C32-1B
Relief valve	BOSH DBETX-1X/315G24-8NZ4M REXROTH DBETX-1X/315024-8MZ4M
Energy storage unit	Maxwell BMOD0165 P048 C01

During the process of the experiment, the engine throttle is fixed and preset as rating speed 1800 rpm. The displacement of the pump and the relief-valve setting pressure are fixed as well. In this test platform, the IPMSM output torque can be calculated as

$$T_a = T_p - T_e \tag{30}$$

where, T_a is the output torque of the IPMSM in the experimental platform. T_p is the absorbed torque of the pump. T_e is the output torque of the engine.

The traditional vector control is also applied to the platform. For different DC supply voltages, the output torque of the IPMSM can be acquired and given in Fig. 16 and Fig. 17. The desired torque of the IPMSM is 200 Nm. The initial DC voltages in Fig. 16 and Fig. 17 are 300 V and 240 V, respectively. It can be found that the control performance of the IPMSM torque will be worse with the decrease of the DC supply voltage. Especially, when the initial DC supply voltage is 240 V, the output torque of the IPMSM is much lower than the desired torque. However, when the DC supply voltage is 300 V, the output torque of the IPMSM is less than 200 Nm. This is mainly because that the torque of the IPMSM is acquired by using the absorbed torque of the pump to subtract the engine output torque. While, there is a great mechanical loss in the HPTS. Even no-load

is added to the pump, the output torque of the engine is greater than 0.

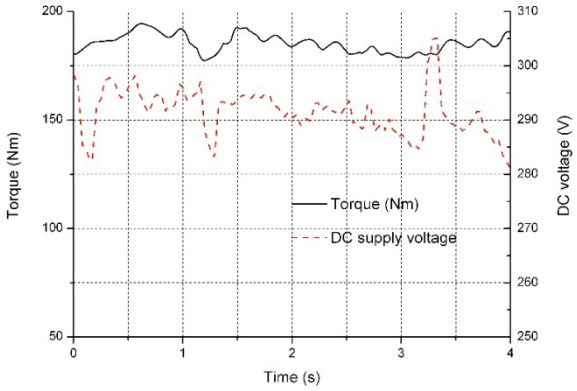

FIGURE 16. The output torque of the IPMSM with traditional control strategy (300 V).

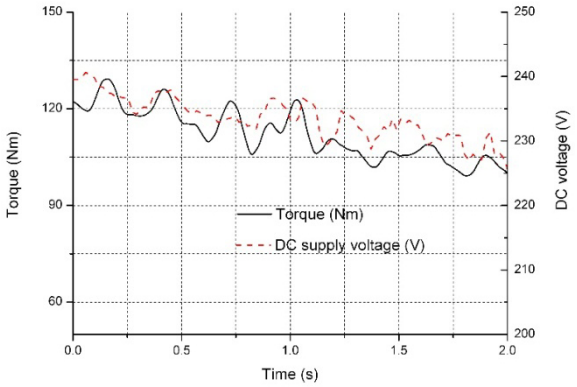

FIGURE 17. The output torque of the IPMSM with traditional control strategy (240 V).

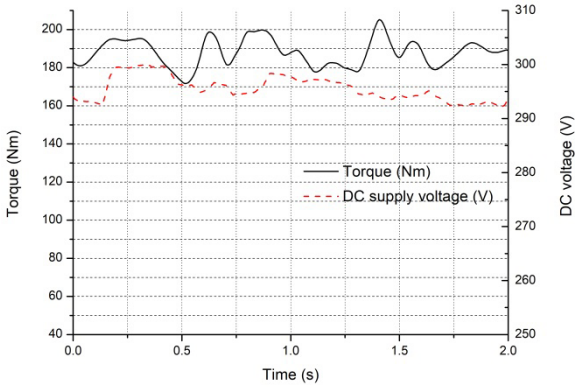

FIGURE 18. The output torque of the IPMSM with high performance control strategy (300 V).

The novel control strategy and same experimental conditions are applied to the platform. The output torque of the IPMSM of different DC supply voltages are given in Fig. 18 and Fig. 19. As can be found, with the decrease of the DC supply voltage, the control performance of the

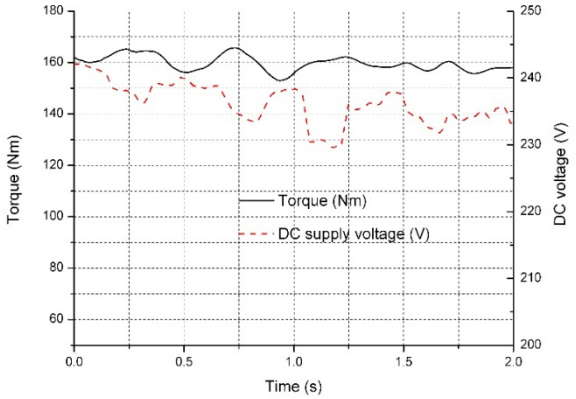

FIGURE 19. The output torque of the IPMSM with high performance control strategy (240 V).

IPMSM output toque is better than that of the traditional vector control.

VII. CONCLUSION

A HPTS is considered as a promising technology to improve the fuel economy of a hydraulic excavator. In the HPTS, an IPMSM is used to balance fluctuations of the load and stabilize working points of the engine in high efficiency area. Ultra-capacitors are used to realize fast charge and discharge. As a result, the DC voltage varies in a wide range. While, the output torque of the IPMSM is affected by the DC supply voltage.

In this paper, a novel control strategy based on a vector control for an IPMSM in the HPTS is proposed so as to reduce the effect from the DC supply voltage on the IPMSM output torque and balance fluctuations of the load adequately. By adopting the novel control strategy, the control performance is improved. Simulations and experiments are carried out to validate the effectiveness of the proposed control strategy.

REFERENCES

[1] M. Kagoshima *et al.*, "Development of new hybrid excavator," *Kobelco Technol. Rev.*, vol. 27, no. 27, pp. 39–42, 2007.
[2] H. Wang, Q. Wang, and B. Hu, "A review of developments in energy storage systems for hybrid excavators," *Autom. Construction*, vol. 80, pp. 1–10, Aug. 2017.
[3] H. Kim, S. Yoo, S. Cho, and K. Yi "Hybrid control algorithm for fuel consumption of a compound hybrid excavator," *Autom. Construction*, vol. 68, pp. 1–10, Aug. 2016.
[4] T. Lin, W. Huang, H. Ren, S. Fu, and Q. Liu, "New compound energy regeneration system and control strategy for hybrid hydraulic excavators," *Autom. Construction*, vol. 68, pp. 11–20, Aug. 2016.
[5] Q. Xiao, Q. Wang, and Y. Zhang, "Control strategies of power system in hybrid hydraulic excavator," *Autom. Construction*, vol. 17, no. 4, pp. 361–367, 2008.
[6] M.-E. Choi, S.-W. Kim, and S.-W. Seo, "Energy management optimization in a battery/supercapacitor hybrid energy storage system," *IEEE Trans. Smart Grid*, vol. 3, no. 1, pp. 463–472, Mar. 2012.
[7] Q. Chen, Q. Wang, and T. Wang, "A novel hybrid control strategy for potential energy regeneration systems of hybrid hydraulic excavators," *Proc. Inst. Mech. Eng. I, J. Syst. Control Eng.*, vol. 230, no. 5, pp. 375–384, 2016.

[8] Z. Chen, B. Yao, and Q. Wang, "μ-synthesis based adaptive robust control of linear-motor-driven stages with high-frequency flexible modes," *IFAC Proceedings Volumes* vol. 46, no. 5, pp. 207–213, 2013.
[9] Z. Chen, Y.-J. Pan, and J. Gu, "Integrated adaptive robust control for multilateral teleoperation systems under arbitrary time delays," *Int. J. Robust Nonlinear Control*, vol. 26, no. 12, pp. 2708–2728, Aug. 2016.
[10] Z. Chen, B. Yao, and Q. Wang, "Accurate motion control of linear motors with adaptive robust compensation of nonlinear electromagnetic field effect," *IEEE/ASME Trans. Mechatronics*, vol. 18, no. 3, pp. 1122–1129, Jun. 2013.
[11] J. Yao, W. Deng, and Z. Jiao, " Adaptive control of hydraulic actuators with lugre model-based friction compensation," *IEEE Trans. Ind. Electron.*, vol. 62, no. 10, pp. 6469–6477, Oct. 2015.
[12] J. Yao, Z. Jiao, and D. Ma, "A practical nonlinear adaptive control of hydraulic servomechanisms with periodic-like disturbances," *IEEE/ASME Trans. Mechatronics*, vol. 20, no. 6, pp. 2752–2760, Dec. 2015.
[13] W. Sun, Y. Zhang, Y. Huang, H. Gao, and O. Kaynak, "Transient-performance-guaranteed robust adaptive control and its application to precision motion control systems," *IEEE Trans. Ind. Electron.*, vol. 63, no. 10, pp. 6510–6518, Oct. 2016.
[14] W. Sun, H. Pan, and H. Gao, "Filter-based adaptive vibration control for active vehicle suspensions with electrohydraulic actuators," *IEEE Trans. Veh. Technol.*, vol. 65, no. 6, pp. 4619–4626, Jun. 2016.
[15] T. Miyajima, H. Fujimoto, and M. Fujitsuna, "A precise model-based design of voltage phase controller for IPMSM," *IEEE Trans. Power Electron.*, vol. 28, no. 12, pp. 5655–5664, Dec. 2013.
[16] M. Preindl and S. Bolognani, "Optimal state reference computation with constrained MTPA criterion for PM motor drives," *IEEE Trans. Power Electron.*, vol. 30, no. 8, pp. 4524–4535, Aug. 2015.
[17] T. Bariša, D. Sumina, and M. Kutija, "Comparison of maximum torque per ampere and loss minimization control for the interior permanent magnet synchronous generator," in *Proc. IEEE Int. Conf. Elect. Drives Power Electron.*, Sep. 2015, pp. 497–502.
[18] G. Pellegrino, E. Armando, and P. Guglielmi, "Direct-flux vector control of IPM motor drives in the maximum torque per voltage speed range," *IEEE Trans. Ind. Electron.*, vol. 59, no. 10, pp. 3780–3788, Oct. 2012.
[19] T. Sun, J. Wang, and M. Koc, "Self-learning direct flux vector control of interior permanent-magnet machine drives," *IEEE Trans. Power Electron.*, vol. 32, no. 6, pp. 4652–4662, Jun. 2017.
[20] L. Tang, L. Zhong, M. F. Rahman, and Y. Hu "A novel direct torque controlled interior permanent magnet synchronous machine drive with low ripple in flux and torque and fixed switching frequency," *IEEE Trans. Power Electron.*, vol. 19, no. 2, pp. 346–354, Mar. 2004.
[21] Y.-S. Choi, H. H. Choi, and J.-W. Jung, "Feedback linearization direct torque control with reduced torque and flux ripples for IPMSM drives," *IEEE Trans. Power Electron.*, vol. 31, no. 5, pp. 3728–3737, May 2016.
[22] M. Koç, J. Wang, and T. Sun, "An inverter nonlinearity-independent flux observer for direct torque-controlled high-performance interior permanent magnet brushless AC drives," *IEEE Trans. Power Electron.*, vol. 32, no. 1, pp. 490–502, Jan. 2016.
[23] H. Ge, Y. Miao, B. Bilgin, B. Nahid-Mobarakeh, and A. Emadi, "Speed range extended maximum torque per ampere control for PM drives considering inverter and motor nonlinearities," *IEEE Trans. Power Electron.*, vol. 32, no. 9, pp. 7151–7159, Sep. 2016.
[24] A. Ahmed, Y. Sozer, and M. Hamdan, "Maximum torque per ampere control for interior permanent magnet motors using DC link power measurement," in *Proc. IEEE Appl. Power Electron. Conf. Expo.*, Mar. 2014, pp. 826–832.

QIHUAI CHEN received the Ph.D. degree in mechatronic engineering from the State Key Laboratory of Fluid Power and Mechatronic Systems, Zhejiang University. In 2016, he joined the College of Mechanical Engineering and Automation, Huaqiao University, where he is involved with a team partner to study construction machinery energy conservation technology. His research interests include the design and control of permanent magnet machines in hybrid power train system, energy regeneration system, and electric power system.

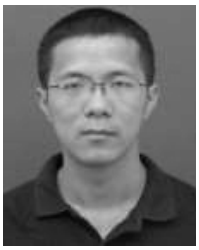

TIANLIANG LIN received the Ph.D. degree in mechatronic engineering from the State Key Laboratory of Fluid Power and Mechatronic Systems, Zhejiang University. In 2016, he joined the College of Mechanical Engineering and Automation, Huaqiao University. He is currently an Associate Professor and the Director of the Department of Mechatronic. His research interests include energy saving technology of electro hydraulic transmission and design of advanced equipment.

HAOLING REN received the M.S. degree in mechatronic engineering from the Harbin Institute of Technology in 2003 and the Ph.D. degree in mechatronic engineering from the State Key Laboratory of Fluid Power and Mechatronic Systems, Zhejiang University, in 2014. She is currently an Associate Director of the Department of Mechatronic, College of Mechanical Engineering and Automation, Huaqiao University. Her research interests are mainly on energy saving technology of electro hydraulic transmission.